

# Assessing 20th century tidal range changes in the North Sea

Leon Jänicke<sup>1</sup>, Andra Ebener<sup>1</sup>, Sönke Dangendorf<sup>2</sup>, Arne Arns<sup>3</sup>, Michael Schindelegger<sup>4</sup>, Sebastian Niehüser<sup>1</sup>, Ivan David Haigh<sup>5</sup>, Philip L. Woodworth<sup>6</sup>, and Jürgen Jensen<sup>7</sup>

<sup>1</sup>Research Institute for Water and Environment, University of Siegen

<sup>2</sup>Old Dominion University

<sup>3</sup>Faculty of Agricultural and Environmental Sciences, University of Rostock

<sup>4</sup>University of Bonn

<sup>5</sup>University of Southampton

<sup>6</sup>National Oceanography Centre

<sup>7</sup>University of Siegen

November 22, 2022

## Abstract

In many places around the world, tide gauges have been measuring substantial non-astronomical changes. Here we document an exceptional large spatial scale case of changes in tidal range in the North Sea, featuring pronounced trends between -2.3 mm/yr in the UK and up to 7 mm/yr in the German Bight between 1958 and 2014. These changes are spatially heterogeneous, suggesting a superposition of local and large-scale processes at work within the basin. We use principal component analysis to separate large-scale signals appearing coherently over multiple stations from rather localized changes. We identify two leading principal components (PCs) that explain about 69% of tidal range changes in the entire North Sea including the divergent trend pattern along UK and German coastlines, which suggest movement of the region's semidiurnal amphidromic areas. By applying numerical and statistical analyses, we can assign a baroclinic (PC1) and a barotropic large-scale signal (PC2), explaining a large part of the overall variance. A comparison between PC2 and tide gauge records along the European Atlantic coast, Iceland and Canada shows significant correlations on time scales of less than 2 years, which suggests an external and basin-wide forcing mechanism. By contrast, PC1 dominates in the southern North Sea and originates, at least in part, from stratification changes in nearby shallow waters. In particular, from an analysis of observed density profiles, we suggest that an increased strength and duration of the summer pycnocline has stabilized the water column against turbulent dissipation and allowed for higher tidal elevations at the coast.

## Assessing 20th century tidal range changes in the North Sea

Leon Jänicke<sup>1</sup>, Andra Ebener<sup>1</sup>, Sönke Dangendorf<sup>2</sup>, Arne Arns<sup>3</sup>, Michael Schindelegger<sup>4</sup>,  
Sebastian Niehüser<sup>1</sup>, Ivan D. Haigh<sup>5</sup>, Philip Woodworth<sup>6</sup> and Jürgen Jensen<sup>1</sup>

<sup>1</sup>Research Institute for Water and Environment, University of Siegen, Siegen, Germany.

<sup>2</sup>Centre for Coastal Physical Oceanography, Old Dominion University, Norfolk, United States of America.

<sup>3</sup>Faculty of Agricultural and Environmental Sciences, University of Rostock, Rostock, Germany.

<sup>4</sup>Institute of Geodesy and Geoinformation (IGG), University of Bonn, Bonn, Germany.

<sup>5</sup>School of Ocean and Earth Science, University of Southampton, Southampton, United Kingdom.

<sup>6</sup>National Oceanography Centre, Liverpool, United Kingdom.

### Key Points:

- 70 North Sea tide gauges evince contrasting trends in tidal range between the UK (-1.0 mm/yr) and the German Bight (3.3 mm/yr) since 1958
- We use principal component analysis (PCA) to separate local (e.g., building measures) from large-scale (e.g., sea level rise) effects
- The first PC explains 77% of variance in the German Bight and is linked to stability changes in shallow, seasonally-stratified waters

### Abstract

In many places around the world, tide gauges have been measuring substantial non-astronomical changes. Here we document an exceptional large spatial scale case of changes in tidal range in the North Sea, featuring pronounced trends between -2.3 mm/yr in the UK and up to 7 mm/yr in the German Bight between 1958 and 2014. These changes are spatially heterogeneous, suggesting a superposition of local and large-scale processes at work within the basin. We use principal component analysis to separate large-scale signals appearing coherently over multiple stations from rather localized changes. We identify two leading principal components (PCs) that explain about 69% of tidal range changes in the entire North Sea including the divergent trend pattern along UK and German coastlines, which suggest movement of the region's semidiurnal amphidromic areas. By applying numerical and statistical analyses, we can assign a baroclinic (PC1) and a barotropic large-scale signal (PC2), explaining a large part of the overall variance. A comparison between PC2 and tide gauge records along the European Atlantic coast, Iceland and Canada shows significant correlations on time scales of less than 2 years, which suggests an external and basin-wide forcing mechanism. By contrast, PC1 dominates in the southern North Sea and originates, at least in part, from stratification changes in nearby shallow waters. In particular, from an analysis of observed density profiles, we suggest that an increased strength

37 and duration of the summer pycnocline has stabilized the water column against turbulent  
38 dissipation and allowed for higher tidal elevations at the coast.

### 39 **Plain Language Summary**

40 Tide gauges in the German Bight show large increases in the tidal range (e.g., difference between  
41 tidal high and tidal low waters) since the mid-1950s, but the causes remain largely unknown.  
42 Here we show that the trends in the tidal range have opposite signs in the southwest and the  
43 southeast of the North Sea, indicating that different causes may be present. Using various novel  
44 analytical methods and numerical modelling, we show that the changes in the southwest are  
45 primarily externally driven by appearing coherently at many sites in the Atlantic Ocean. In  
46 contrast, tidal range variability in the German Bight seem to be linked with changes in local  
47 stratification of the North Sea.

### 48 **1 Introduction**

49 For thousands of years, tides have had a great influence on coastal areas globally and their  
50 residents. Today they play a critical role in influencing economic considerations, nautical safety,  
51 renewable energy schemes, assessments of land erosion, and the definition of geodetic datums  
52 (Haigh et al., 2020; Pugh & Woodworth, 2014). Tides not only control the navigability of some  
53 ports and sea routes, but also have a major influence on the intensity and timing of extreme sea  
54 levels during storm surges (e.g., Arns et al., 2020; Horsburgh & Wilson, 2007; Prandle & Wolf,  
55 1978). Given their close connection to the periodic and predictable nature of astronomical  
56 variations, the amplitudes and phases of tidal constituents, and corresponding tidal water levels,  
57 are generally assumed to be constant on time scales over which basin geometry undergoes only  
58 minor changes (i.e., decades to centuries). However, Keller (1901) showed increased tidal  
59 amplitudes due to reflection and local resonance changes as a result of building measures such as  
60 weirs (e.g., in the Ems River). Similarly Doodson (1924) pointed to appreciable secular  
61 perturbations in the local tidal regimes of particular ports, weirs, and estuaries. More recently,  
62 the topic of changes in ocean tides has been revived and extended to the scales of shelves, basins  
63 and the global ocean – a development fueled by the digitization and publication of global data  
64 sets of tide gauge records, see Woodworth et al. (2017). In fact, statistically significant trends of  
65 tidal parameters of the order of a few percent (in relative terms) are now well documented  
66 around the world (e.g., Flick et al., 2003; Jay, 2009; Mawdsley et al., 2015; Ray, 2009; Talke &  
67 Jay, 2017; Woodworth et al., 1991;). Fluctuations of similar magnitude and regional extent have  
68 been observed on interannual time scales (e.g., Devlin et al., 2014; Feng et al., 2015; Müller,  
69 2011; Ray & Talke, 2019).

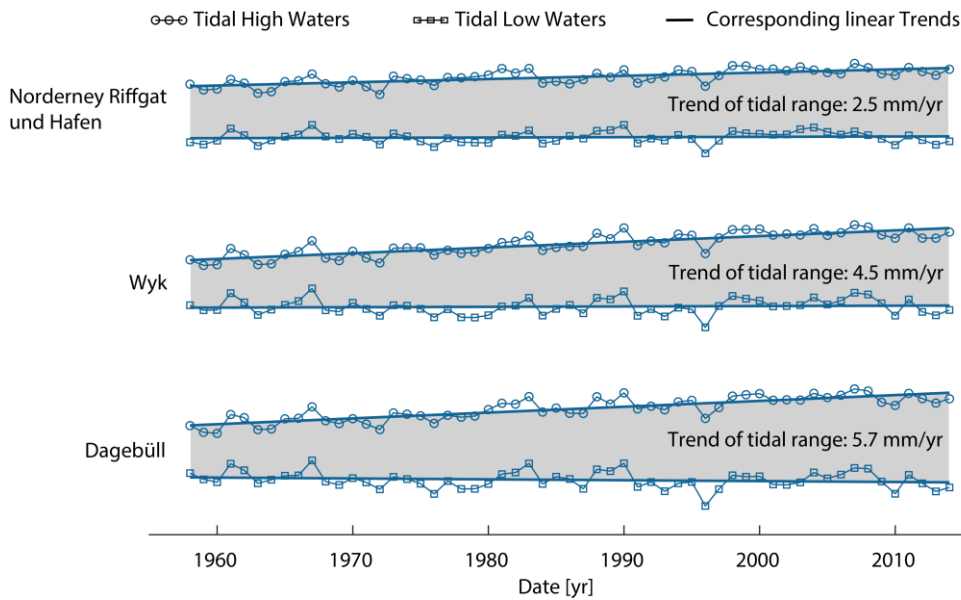
70 Despite this ample evidence of changes in tides in water level series, the forcing factors and  
71 spatial extent of secular and short-term variability in tides remain uncertain. Woodworth (2010)  
72 succeeded in detecting coherent patterns of amplitude and phase trends in primary constituents  
73 along the North American coasts, but found less regional consistency in data from Asia, the  
74 Australian Seas or Europe. However, some spatially coherent changes could still be observed in

75 smaller and well-instrumented areas. A major problem identified by Woodworth (2010) is that  
76 small-scale (often site-specific) and large-scale changes may occur simultaneously, thereby  
77 impeding research of the underlying physical processes. Over wider coastal sections, and at sites  
78 open to the sea, the effects of a rise in mean sea level (MSL) on tidal wave propagation explain  
79 only a fraction of the observed trends (Müller et al., 2011; Schindelegger et al., 2018).  
80 Accordingly, the assumption persists that other mechanisms – such as changes in stratification,  
81 turbulent dissipation, and variations in shoreline position or bed roughness – play major roles;  
82 see Haigh et al. (2020) for a review. The present consensus is that in many areas of the world a  
83 combination of different oceanographic processes may be at work. For instance, Ray & Talke  
84 (2019) suggest that the large secular changes of the lunar  $M_2$  tide in the Gulf of Maine could be  
85 caused by both sea level rise and persistent stratification changes. Yet, as implied above, any  
86 contributing mechanism will act on its own characteristic spatial and temporal scales, overlaying  
87 and possibly reinforcing other processes. This particularly applies to anthropogenic construction  
88 measures (e.g., building of dykes and tidal barriers) that can cause transient perturbations to the  
89 local tidal regime and affect adjacent stretches of coastline (Talke & Jay, 2020). Therefore, a  
90 major challenge is the separation of local effects and large-scale changes and their subsequent  
91 attribution to certain forcing factors.

92 Exceptional changes in tidal range are found in the German Bight, documented in Führböter &  
93 Jensen (1985) and Jensen (2020). Between 1958 and 2014, different changes in tidal range were  
94 detected ranging from approximately 3% at some of the investigated tide gauges to more than  
95 11% at others (Figure 1). The latter is equivalent to a trend of 5.7 mm/yr and outpaces the  
96 simultaneous local (Dangendorf et al., 2015) and global MSL rise (Dangendorf et al., 2019;  
97 Oppenheimer et al., 2019). To our knowledge, this magnitude of tidal range change is one of the  
98 highest in the world, only exceeded by developments in the Gulf of Maine (Ray & Talke, 2019).  
99 It further seems that the overlap between local and large-scale effects in the North Sea is  
100 particularly pronounced, possibly nurtured by the region's character as a shelf sea with a tide  
101 generated in the Atlantic. Previous research (summarized in Jensen et al., 2014) has ruled out  
102 astronomical, large-scale morphological or tectonic causes (at least in the German Bight), but  
103 pointed to the generally non-linear and non-uniform behavior of water levels in the North Sea.  
104 To improve our understanding of these puzzling tidal range changes, we aim to address the  
105 following questions through systematic data analysis: (1) Are these changes on different time  
106 scales detected within the German Bight a localized phenomenon, or are they part of a larger-  
107 scale development spreading over larger areas within or even outside the North Sea region? (2)  
108 Is it possible to separate and quantify large-scale and small-scale effects from observed records?  
109 (3) If (2) is the case; can we attribute physical causes to the observed changes?

110 Below, we first discuss geographic and oceanographic characteristics that are fundamental to the  
111 understanding of the tidal regime in the North Sea, the available database, its limitations and  
112 major processing steps (Section 2). Section 3 introduces the analytical methods of Ordinary  
113 Kriging, which is here mainly used for gap-filling as the following PCA requires complete time

114 series. The results of our analyses are described extensively in Section 4. To answer the  
 115 abovementioned research questions, we start our analyses with the detection of observed changes  
 116 in the tidal range at individual sites. In a second step, we apply a PCA to identify modes of  
 117 variability common to all (or the majority of) sites and to distinguish them from local anomalies.  
 118 In a last step we analyze potential causes and drivers of the observed changes. The paper  
 119 concludes with a summary and additional remarks in Section 5.  
 120



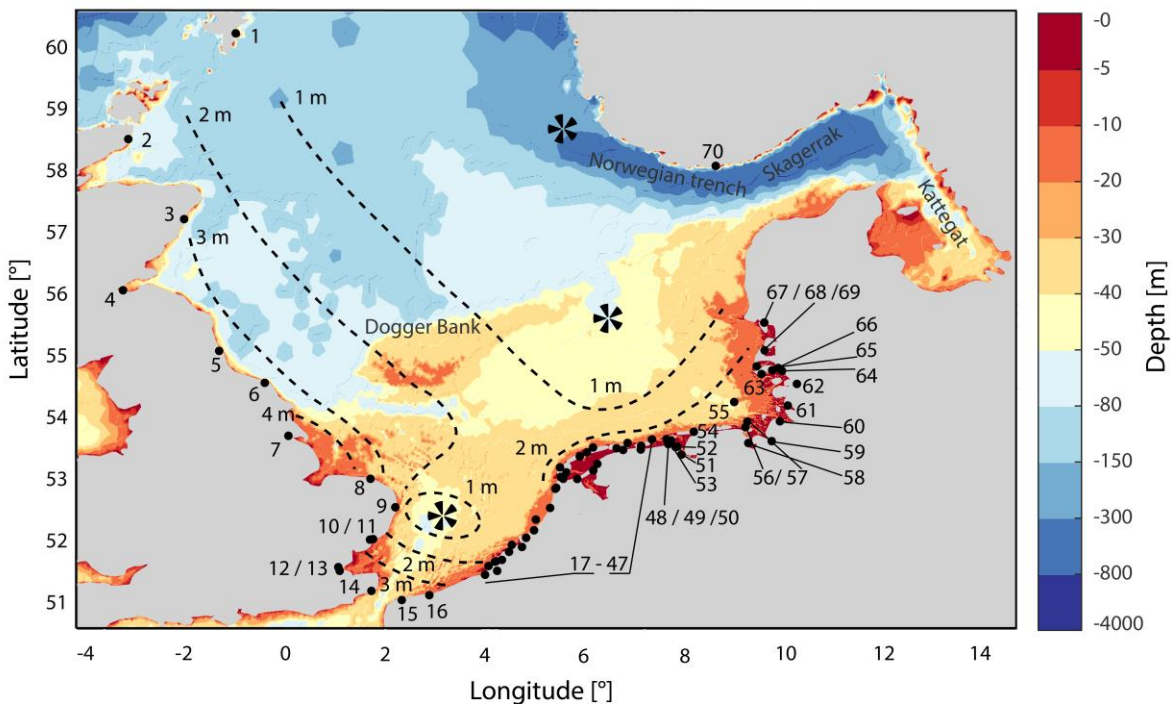
121  
 122 Figure 1: Time series of mean annual high and low tidal water levels for three exemplarily selected stations in the  
 123 German Bight. For illustration purposes all records are shown with different artificial vertical offsets. The increase  
 124 in the tidal range is illustrated for the three sites as grey shaded areas between high and low water level time series.

125 **2 Study area and data basis**

126 **2.1 Study area**

127 The North Sea is one of the largest shelf seas on Earth with a size of about 575.300 km<sup>2</sup>  
 128 (Huthnance, 1991). Counted counter-clockwise, its margins comprise coastal sections of the  
 129 United Kingdom, France, Belgium, the Netherlands, Germany, Denmark and the south of  
 130 Norway (Figure 2). The North Sea is connected to the North Atlantic via a large inlet between  
 131 Scotland and Norway in the north and a narrow opening through the English Channel in the  
 132 southwest and it opens to the Baltic Sea in the east. Water depths in the North Sea are on average  
 133 90 m but vary greatly, generally increasing from south to north. While the southern parts are  
 134 often shallower than 40 m with lowest depths in the German Bight, they increase to about 300 m  
 135 at the continental shelf toward the Norwegian Trench and toward the entry into the Norwegian  
 136 Sea in the northwest. There are also extensive shallow water regions off the south-eastern coast  
 137 of the UK known as the Dogger Bank complex, with their western part extending to the coasts of  
 138 Norfolk and Suffolk (Quante & Colijn, 2016).

139 The tidal regime in most parts of the North Sea is strongly influenced by the astronomical tides  
 140 entering the basin from the Atlantic and therefore mainly semidiurnal. The greater part of these  
 141 oscillations enters between the Shetlands and Scottish mainland and a smaller part through the  
 142 English Channel. They travel counter-clockwise through the entire North Sea basin as Kelvin  
 143 waves. The entry times of the tidal high and low waters are therefore shifted relative to each  
 144 other according to the celerity of the tidal wave. This physical setting results in three  
 145 amphidromic points, one close to the English Channel, one off the coast of Norway and one  
 146 central in the North Sea basin (Proudman & Doodson, 1924). Since the North Sea's basin shape  
 147 is close to the resonance frequency in the semidiurnal spectral band, the superposition of the  
 148 principal lunar and solar tides  $M_2$  and  $S_2$  leads to a significant spring neap cycle. These two  
 149 constituents cause a potential tidal range between 1 and 5 m (Quante & Colijn, 2016).  
 150 Accordingly, the tidal regime of the North Sea can be classified as macrotidal ( $>4$  m), mesotidal  
 151 (2-4 m) and microtidal ( $<2$  m) (Haigh, 2017), with the actual tidal range being strongly  
 152 influenced by local factors. For example, the mean spring tidal range at the east coast of the UK  
 153 varies between 3.60 m (Aberdeen) and 6.20 m (Immingham) (Horsburgh & Wilson, 2007). The  
 154 mean tidal range in the data set used below is about 3.40 m in the UK and the English Channel,  
 155 1.98 m at the Dutch west coast, 2.33 m at the Dutch north coast and 2.82 in the German Bight.



156  
 157 Figure 2: Bathymetry of the North Sea (Becker et al., 2009; Schrottko & Heyer, 2013). Also shown are the locations  
 158 of tide gauges (black dots) used in this study including their respective numbering (see also Table 1). The black  
 159 propellers indicate the location of the three semidiurnal amphidromic areas (including the amphidromic points for  
 160 the  $M_2$  and  $S_2$  constituent) and the black dotted lines indicate contours of equal mean tidal range (Sündermann &  
 161 Pohlmann, 2011).

162

163 **2.2 Data**

164 Time series of water level from 70 available tide gauges around the North Sea basin were  
 165 collected from various sources. Data from GESLA (Global Extreme Sea Level Analysis,  
 166 GESLA, Woodworth et al. 2017), Open Earth (Deltares) and the responsible German authorities  
 167 (Wasser- und Schifffahrtsverwaltung des Bundes via the portals of the associated Central Data  
 168 Management, ZDM) were used. The available time series vary considerably in length and  
 169 completeness. The earliest measurements in the form of tidal high and low water readings are  
 170 from 1843 (the tide gauge at Cuxhaven Steubenhöft, Germany), while on the Dutch coast data  
 171 from some stations have only been digitally available since the 1980s. High-resolution data sets  
 172 with an equidistant sampling between 1 and 60 minutes were used as well as time series of tidal  
 173 high and low water. We excluded equidistant time series with a resolution lower than 60  
 174 minutes, as supplemental analyses have shown that they insufficiently describe the height and  
 175 timing of individual tidal high and low waters. The tidal range was calculated as the difference  
 176 between each tidal high water and the mean of the two surrounding tidal low waters, according  
 177 to the German standard (DIN 4049-3, 1994). From those, we calculated monthly averages and  
 178 removed the mean seasonal cycle, as we are mainly interested in longer-term changes.  
 179 Considering the 18.6-year nodal cycle and the end of numerous water level series in December  
 180 2014, we adopt an analysis period from January 1958 to December 2014; approximately 3 nodal  
 181 cycles. Tide gauges known to be located near to weir installations or in rivers were excluded, as  
 182 these are at least partially separated from the oscillation system of the North Sea. Seventy time  
 183 series of tidal range remained in the data set, forming the basis for our investigations (Table 1,  
 184 Figure 2 and Figure 3). Acknowledging the counter-clockwise propagation direction of the tidal  
 185 wave, the tide gauges used in this study are counted by starting at Lerwick (Shetland Islands) and  
 186 ending at Tregde (Norway). The average completeness of the stations is 64% in the UK, 65% in  
 187 the Netherlands and around 88% in Germany.

188 Table 1: Name, coordinates, period and coverage of the 70 tide gauges used in this study (see also Figure 2).

<b>Tide gauge</b>	<b>Lon. [°]</b>	<b>Lat. [°]</b>	<b>Period [yr]</b>	<b>Cov. [-]</b>	<b>Tide gauge</b>	<b>Lon. [°]</b>	<b>Lat. [°]</b>	<b>Period [yr]</b>	<b>Cov. [-]</b>
1 Lerwick	-1.14	60.16	1959 – 2011	0.83	36 Kornwerderzandbuiten	5.34	53.07	1958-2014	1.00
2 Wick	-3.09	58.44	1965 – 2014	0.79	37 Texel Noordzee	4.73	53.12	1990 – 2014	0.27
3 Aberdeen	-2.07	57.14	1958 – 2014	0.75	38 Harlingen	5.41	53.18	1958 – 2014	1.00
4 Leith	-3.18	55.99	1989 – 2014	0.39	39 Vlielandhaven	5.09	53.3	1958 – 2014	1.00
5 North Shields	-1.44	55.01	1962 – 2014	0.79	40 West-Terschelling	5.22	53.36	1958 – 2014	1.00
6 Whitby	-0.61	54.49	1981 – 2014	0.55	41 Terschelling Noordzee	5.33	53.44	1989 – 2014	0.45
7 Immingham	-0.19	53.63	1958 – 2014	0.90	42 Nes	5.76	53.43	1971 – 2014	0.77
8 Cromer	1.30	52.93	1988 – 2014	0.45	43 Holwerd	5.88	53.4	1971 – 2014	0.54
9 Lowestoft	1.75	52.47	1964 – 2014	0.86	44 Wierumergronden	5.96	53.52	1981 – 2014	0.60
10 Felixstowe	1.35	51.96	1982 – 2011	0.39	45 Lauwersoog	6.20	53.41	1971 – 2014	0.77
11 Harwich	1.29	51.95	1958 – 2014	0.29	46 Schiermonnikoog	6.20	53.47	1966 – 2014	0.86
12 Southend	0.72	51.5	1958 – 1981	0.40	47 Huijbertgat	6.40	53.57	1973 – 2014	0.74
13 Sheerness	0.74	51.44	1958 – 2013	0.64	48 Borkum Fischerbalje	6.75	53.56	1963 – 2014	0.90

14	Dover	1.32	51.12	1958 – 2014	0.90	49	Borkum Südstrand	6.66	53.58	1958 – 2014	1.00
15	Calais	1.87	50.97	1965 – 2014	0.52	50	OudeWestereems	6.70	53.5	1981 – 1983	0.04
16	Dunkerque	2.37	51.05	1959 – 2014	0.68	51	Eemshaven Doekegat	6.86	53.46	1983 – 1987	0.07
17	Cadzand	3.38	51.38	1971 – 2014	0.77	52	Eemshaven	6.83	53.45	1979 – 2014	0.63
18	Westkapelle	3.44	51.52	1958 – 2014	1.00	53	Delfzijl	6.93	53.33	1958 – 2014	1.00
19	Oostkapelle	3.56	51.59	1971 – 2014	0.77	54	Norderney Riffgat und Hafen	7.16	53.7	1958 – 2014	1.00
20	Oranjezon	3.57	51.6	1979 – 1987	0.14	55	Helgoland Binnenhafen	7.89	54.18	1958 – 2014	1.00
21	Roompot- buiten	3.68	51.62	1972 – 1974	0.04	56	LT Alte Weser – Roter Sand	8.13	53.86	1958 – 2014	1.00
22	Brouwers- havenscheGat0 8	3.81	51.75	1987 – 2014	0.49	57	Wilhelmshaven Alter Vorhafen	8.15	53.51	1958 – 2014	1.00
23	Haringvliet10	3.86	51.86	1980 – 2014	0.61	58	Bremerhaven	8.57	53.55	1958 – 2014	1.00
24	Haringvliets- luizenbuiten	4.04	51.83	1982 – 2014	0.54	59	Mellumplate	8.09	53.77	1963 – 2014	0.91
25	Hoek van Holland	4.12	51.98	1972 – 1987	0.26	60	Cuxhaven Steubenhöft	8.72	53.87	1958 – 2014	1.00
26	Scheveningen	4.26	52.1	1958 – 2014	1.00	61	Büsum	8.86	54.12	1958 – 2014	1.00
27	Noordwijk- meetpost	4.30	52.27	1961 – 2005	0.76	62	Husum	9.02	54.47	1958 – 2014	1.00
28	Ijmuiden- buitenhaven	4.55	52.46	1984 – 2006	0.36	63	Wittdün	8.38	54.63	1958 – 2014	1.00
29	Pettenzuid	4.65	52.77	1981 – 2014	0.60	64	Schlüttsiel	8.76	54.68	1961 – 2014	0.94
30	Petten	4.66	52.79	1978 – 2014	0.61	65	Wyk auf Föhr	8.58	54.69	1958 – 2014	1.00
31	Den Helder	4.74	52.96	1971 – 1974	0.05	66	Dagebüll	8.69	54.73	1958 – 2014	1.00
32	Oostoever	4.79	52.93	1958 – 2014	1.00	67	Hörnum	8.30	54.76	1958 – 2014	1.00
33	Den Oeverbuiten	5.05	52.93	1971 – 1981	0.15	68	List	8.44	55.02	1958 – 2014	1.00
34	Oudeschild	4.85	53.04	1958 – 2014	1.00	69	Esbjerg	8.43	55.47	1958 – 2014	0.92
35	Vlissingen	3.60	51.44	1958 – 2014	1.00	70	Tregde	7.55	58.01	1958 – 2014	0.40

189

190 The statistical analyses and procedures (Ordinary Kriging, Trend analysis, PCA) carried out here  
 191 are based exclusively on the tide gauge records named in Table 1. In Section 4.4 the possible  
 192 correlation between the records from the North Sea and the adjacent North Atlantic is examined.  
 193 For this purpose, 24 additional North Atlantic tide gauges from the GESLA dataset were used  
 194 (Port-aux-Basques, Argentia, Saint John, Reykjavik, Cascais, Vigo, La Coruna, Santander, Saint  
 195 Jean de Luz, Bayonne Boucau, Port Bloc, Les Sables D'Olonne, Saint Gildas, Port Tudy, Brest,  
 196 Le Conquet, Newlyn, Roscoff, Devonport, Saint-Malo, Cherbourg, Le Havre, Newhaven and  
 197 Dieppe, Woodworth et al., 2017).

### 198 3 Methodology

199 In addition to the procedures explained in the following sections, linear trend analysis, harmonic  
 200 analysis of tidal constituents and wavelet coherence analysis were carried out to characterize  
 201 multiple feature of the tide gauge records in the North Sea. Any significance statements made  
 202 throughout the manuscript are based on a 95% confidence level. We calculated linear trends  
 203 using ordinary least squares regression and assessed their significance by considering normally

204 distributed but serially correlated residuals following an autoregressive process of the order 1  
 205 (e.g., Mawdsley & Haigh, 2016). Annual amplitudes for the leading constituents were  
 206 determined by a harmonic analysis using the MATLAB toolbox U-Tide (Codiga, 2011) and the  
 207 wavelet analyses were conducted with the MATLAB package of Grinsted et al. (2004). None of  
 208 these methods are explained here in detail due to their general recognition and widespread use.

209 Furthermore, an existing barotropic tide and surge model of the North Sea and the adjacent  
 210 Atlantic Ocean developed by Arns et al. (2015a, b) was updated and used to simulate total water  
 211 levels from 1958 to 2014. At the open boundaries, we used the Technical University of Denmark  
 212 DTU10 ocean tide model (Cheng & Andersen, 2010) as tidal input, and the MSL reconstructions  
 213 of Wahl et al. (2013) were employed in order to incorporate the effects of rise in MSL. The  
 214 entire model domain was forced with the 20th Century Reanalysis (20CR) data set of the US  
 215 National Oceanic & Atmospheric Administration (NOAA) and the Cooperative Institute for  
 216 Research in Environmental Sciences (CIRES) to describe the meteorologically induced effects  
 217 on water levels (Compo et al., 2011).

### 218 **3.1 Kriging**

219 Kriging (also Gaussian process regression) is a geostatistical method to interpolate missing  
 220 values based on information stemming from neighboring stations (i.e. their covariance matrix). It  
 221 is here mainly used for gap-filling as the following Principal Component Analysis (PCA)  
 222 requires complete time series. Originally developed in the 1950s for mining purposes (Kriging,  
 223 1951), this method has been used increasingly in other areas including the analysis and  
 224 interpretation of incomplete surface air temperature fields (Rigor et al., 2000; Rohde et al.,  
 225 2013). In general, Kriging is a linear interpolation procedure. Missing values are determined  
 226 according to a given covariance matrix, which is calculated from the existing observations  
 227 (Cressie, 1990). Kriging provides some important advantages over other interpolation  
 228 procedures. The interpolated values change smoothly and always pass through the observed  
 229 values at the sample points. Problems related to the accretion of measurement points are avoided  
 230 by considering the statistical distances between the neighbors used in the interpolation of a  
 231 certain value, which means that the spatial variance is taken into account. If clustering occurs in  
 232 a region, the weights of the affected sample points are reduced by including the density. In sparse  
 233 regions, only the distance is considered. The procedure can be summarized with the formula

$$234 \hat{Z}_{(x_0)} = [w_1 \ w_2 \ \dots \ w_{n-1} \ w_n] \cdot \begin{bmatrix} z_1 \\ z_2 \\ \vdots \\ z_{n-1} \\ z_n \end{bmatrix} = \sum_{i=1}^n w_i(x_0) \times Z(x_i), \quad (\text{Eq. 1})$$

235 where  $\hat{Z}$  is the query value at the unobserved location  $x_0$  and  $i = 1 \dots n$  represents a running  
 236 index over  $n$  observations.  $\hat{Z}$  is computed from a linear combination of all observed values  
 237  $z_i = Z(x_i)$ , which are weighted by the parameter  $w$  according to distance and density. A special  
 238

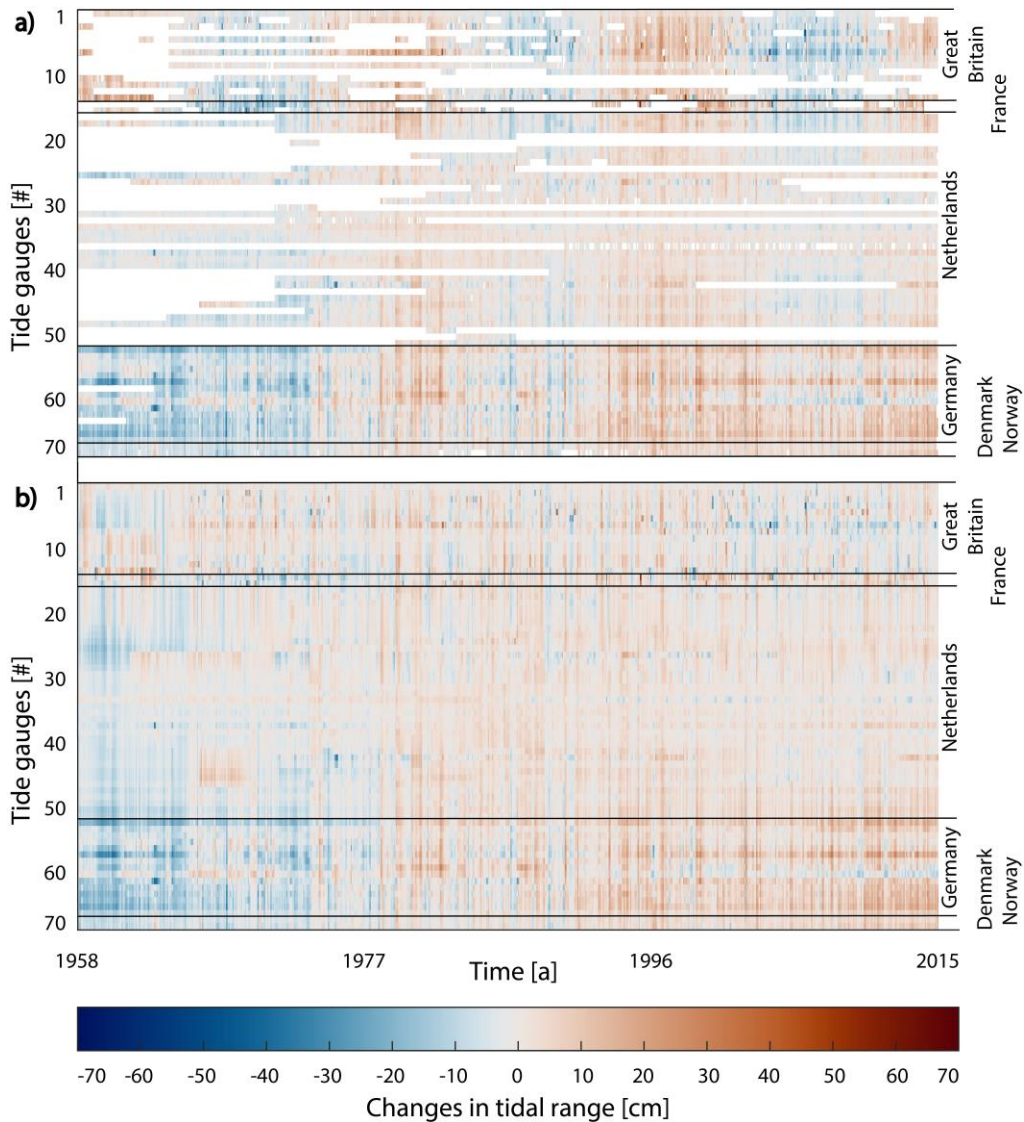
239 property of the Kriging procedure is the convergence of interpolated values to the mean value of  
240 their region with increasing distance to the available samples. That is why Kriging estimates at  
241 query points tend to be conservative (Cowtan & Way, 2014). In keeping with this characteristic,  
242 the general tidal range behavior worked out later in Section 4.1 is also valid when the Kriging  
243 step is omitted.

244

245 We use Kriging for two different purposes. First, the temporal gaps in the tidal range data  
246 (Section 2.2) were closed for each monthly time step in the investigation period. Figure 3-a  
247 illustrates that this is a relevant issue in the Netherlands, in particular before 1970, while in the  
248 UK data gaps occur before 1990. Second, additional data points along the coastline of the North  
249 Sea were interpolated, allowing us not only an analysis of the temporal evolution of each station  
250 series in terms of a linear trend but also a spatial analysis of the different developments (Figure  
251 4). For both applications, we use the Ordinary Kriging algorithm of Schwanghart (2020). Note  
252 also that in transitioning from Figure 3-a to Figure 3-b, the nodal cycle (with peaks for  
253 semidiurnal  $M_2$  in the years 1977, 1996, and 2015) was removed.

254

255



256

257 Figure 3: Changes in tidal range before (a) and after (b) applying ordinary kriging and removing the nodal cycle.

258 **3.2 Principal Component Analysis**

259 Principal Component Analysis (PCA), a method of multivariate statistics, is used to structure and  
 260 simplify extensive data sets by approximating a large number of statistical variables with a  
 261 smaller number of significant, non-correlated (orthogonal) linear combinations. If  $x$  is a vector  
 262 with  $n$  random variables, first a linear function  $f_1(x)$  – dependent on constant coefficients  $c_{1i}$  – is  
 263 determined by calculating the eigenvector from the spatially weighted covariance matrix of  $x$ .  
 264 Then  $f_1(x)$  represents the largest possible overall variance of all variables in  $x$ :

265

$$f_{1(x)} = c_{11} \cdot x_1 + c_{12} \cdot x_2 + \dots + c_{1n-1} \cdot x_{n-1} + c_{1n} \cdot x_n = \sum_{i=1}^n c_{1i} \cdot x_{1i} \quad (\text{Eq. 2})$$

266

267 This decomposition process is repeated for a function  $f_{2(x)}$ , which is uncorrelated with  $f_{1(x)}$  and  
268 describes the largest possible amount of the remaining variance. It is possible to find  $n$  such  
269 functions, but the purpose is usually to explain as much variance as possible with significantly  
270 fewer functions  $f_{i(x)}$ , known as Principal Components (PCs) (Jolliffe, 2002). Therefore, the PC  
271 of a temporally and/or spatially varying physical process represents orthogonal spatial patterns,  
272 in which the data variance is concentrated. Using the leading PC, an approximate reconstruction  
273 of the observed variable can be generated. This type of analysis is often used in Earth system  
274 sciences to identify spatial and temporal patterns of climate oscillations.

275

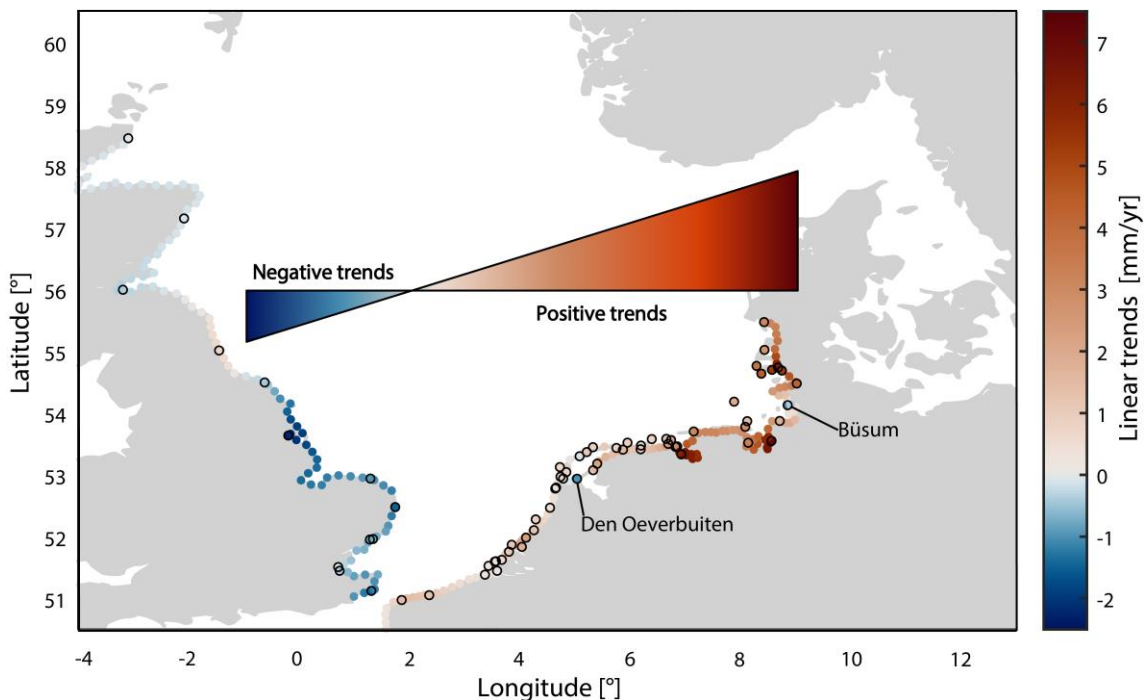
276 In this study, we apply PCA to the entire monthly de-seasoned tidal range data set from the 70  
277 sites (Figure 2), whose gaps were previously filled through Ordinary Kriging. If there are indeed  
278 large-scale signals affecting the tidal range in the North Sea, they should appear as a coherent  
279 pattern visible at multiple sites, and therefore be visible in the leading PCs. By contrast, spatially  
280 confined (“small-scale”) anomalies in tidal range will be shifted into the higher PCs, as these can  
281 only be responsible for a small part of the overall variance. Such shifting includes not only the  
282 response of the local tidal system to, for instance, anthropogenic construction measures but also  
283 to changes in bathymetry or morphology. Local effects can explain more variance than large-  
284 scale effects at individual sites or small subsets, but never for the entire data set. It is therefore  
285 important to consider the explained variance of the PCs at each tide gauge individually to ensure  
286 that large-scale effects with a very small influence on the overall variance are retained. With this  
287 approach, the PCA enables us not only to attribute tidal range changes to small-scale and large-  
288 scale effects, but also to calculate the spatial extent and the temporal development of patterns  
289 that might reflect important environmental factors.

## 290 **4 Results and Discussion**

### 291 **4.1 Trends of tidal range and tidal constituents**

292 To address the three research questions defined in the introduction, we first map the spatial  
293 extent of the long-term changes in tidal range in the study area. We start our analysis by  
294 calculating linear trends for each individual record over a common period between 1958 and  
295 2014 and map them in Figure 4. In this step of the analysis, the time series of Lerwick (Shetland  
296 Islands) and Tregde (Norway) were omitted, since both are the only available tide gauges within  
297 large areas and, therefore, there is not a sufficient data density for use by the Kriging algorithm.  
298 We identify a variety of trends with a particularly pronounced spread in the southern parts of the  
299 basin. While there are no significant trends at the north-eastern coast of the UK, negative trends  
300 occur further south between Immingham and Dover. Here, six of eight stations show significant  
301 negative trends while the remaining two do not differ significantly from zero. In this area,  
302 Immingham shows the largest negative and statistically significant trend ( $-2.3 \pm 0.5$  mm/yr) of all  
303 sites, while the smallest negative trend of  $-0.7 \pm 0.3$  mm/yr is found in Felixstowe. The mean  
304 value for all tide gauges in this area is  $-1.0$  mm/yr. In contrast, trends turn positive on the

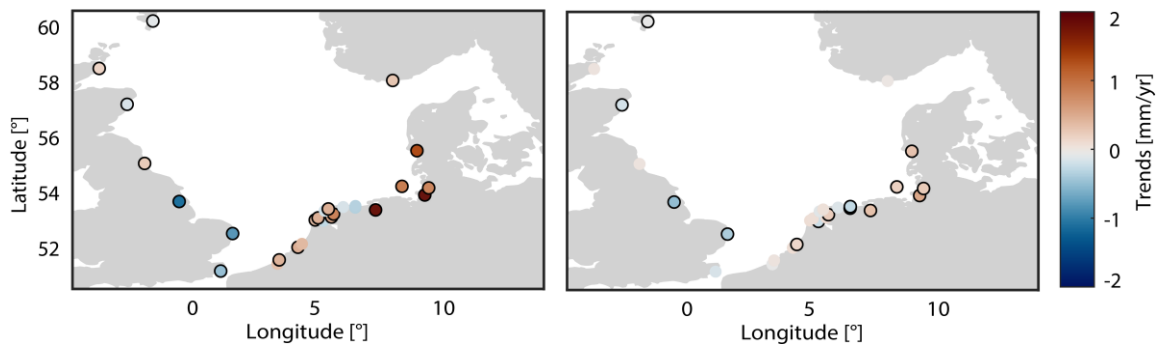
305 continental side of the English Channel and the European West Coast. Our assessment reveal  
 306 increasing trends following the coastlines of France (trend at tide gauge Dunkerque  $1.3 \pm 0.4$   
 307 mm/yr), Belgium and the western Netherlands up to the tide gauge at Huibertgat ( $0.8 \pm 0.2$   
 308 mm/yr), near to the German-Dutch border. On average, trends along the European West Coast  
 309 are 0.8 mm/yr. Hereafter, sharp trend increases are found within a short distance, reaching values  
 310 of more than 7 mm/yr in the German Bight area. Here, the average trend in tidal range amounts  
 311 to 3.3 mm/yr (Table 2). Local changes affect some tide gauges like Den Oeverbuiten  
 312 (Netherlands) or Büsum (Germany), which at first sight seem to contradict this spatial pattern.  
 313 We suggest that these local exceptions are mainly caused by anthropogenic interventions such as  
 314 the building of the Afsluitdijk at Den Oeverbuiten or dredging and dike constructions near to  
 315 Büsum, as they provide different evidence to nearby stations and anomalies in their time series of  
 316 tidal range coincide with known local anthropogenic interventions. From the aforementioned  
 317 findings, we conclude that widespread and statistically significant secular changes in tidal range  
 318 occurred around large parts of the southern North Sea between 1958 and 2014, although locally  
 319 interrupted by opposing signals at individual sites. Furthermore, we note contrasting and dipole-  
 320 like trends along south-western (significant negative values) and south-eastern margins of the  
 321 North Sea (significant positive values). It remains to be critically noted that the changes in the  
 322 tidal range at some individual tide gauges could also be instrumental. However, due to the large-  
 323 scale and the spatial homogeneity of the patterns, this cannot be causal for the overall picture.  
 324



325  
 326 Figure 4: Linear trends of tidal range between 1958 and 2014. Trends at measured sites are shown as dots with a  
 327 black edge. Dots in between stations are based on Kriging.

328 The identified dipole-like trend pattern has its node approximately at the longitude of the English  
 329 Channel (Figure 4) and suggests a westward displacement of the main low amplitude areas  
 330 (including amphidromic points of  $M_2$  and  $S_2$ ) located in the central North Sea and near the  
 331 English Channel (Figure 2). To obtain further indications of such a shift, we perform a harmonic  
 332 analysis to determine the main semi-diurnal  $M_2$  and  $S_2$  tidal constituents, which make the largest  
 333 contributions to the tides in the North Sea. Since high-resolution hourly time series with a  
 334 coverage of at least 75% between 1958 and 2014 are required for a tidal analysis, only a subset  
 335 of 28 tide gauge records is appropriate for our assessment. The available database is thus reduced  
 336 and fewer stations show significant trends (20 for  $M_2$ , 14 for  $S_2$ ). Nevertheless, the overall  
 337 finding (Figure 5) are similar to the assessment focusing on tidal ranges highlighted in Figure 4;  
 338 that is for both constituents (though with larger magnitude for  $M_2$ ), negative trends occur in the  
 339 southeast of the UK and the highest positive trends are found in the German Bight area. A  
 340 displacement of the  $M_2$  and  $S_2$  amphidromic point is, therefore, also inferred.

341



342

343 Figure 5: (a) Linear trends of the  $M_2$  and (b)  $S_2$  tidal constituents between 1958 and 2014 (significant trends  
 344 outlined).

345 Basically, the observed changes in tidal range correspond to the ideas of Taylor (1922). Taylor  
 346 showed analytically that an altered propagation speed due to increased water depth can lead to a  
 347 shift of the amphidromic point in a semi-enclosed basin towards the open boundary. Haigh et al.  
 348 (2020) pointed out the importance of friction and dissipation effects that were not considered by  
 349 Taylor (1922). While MSL rise in a semi-enclosed basin like the North Sea should lead  
 350 principally to a shift of the amphidromic point towards the open boundary and therefore towards  
 351 the north, the associated change in tidal currents and thus the spatial patterns of dissipation may  
 352 alter this effect. For the North Sea, increased frictional dissipation would cause a shift of the  
 353 amphidromic point towards the west, that is, a reduction of the tidal range on the left side of  
 354 Figure 4 (i.e. the east coast of the UK) and an increase on the right side of the basin (i.e. the  
 355 German Bight). This argument is supported by several numerical modelling efforts (Idier et al.,  
 356 2017; Pickering et al., 2012; Schindelegger et al., 2018), in which the impact of large (0–10 m)  
 357 MSL increases on leading constituents (mainly  $M_2$ ) were investigated. Complementary to our  
 358 empirical assessment, they all detected (at least qualitatively) similar patterns as shown in Figure  
 359 4 and 5. However, closer examination also reveals some discrepancies and the model results do  
 360 not correspond exactly to the measured data. For instance, both Pickering et al. (2012) and

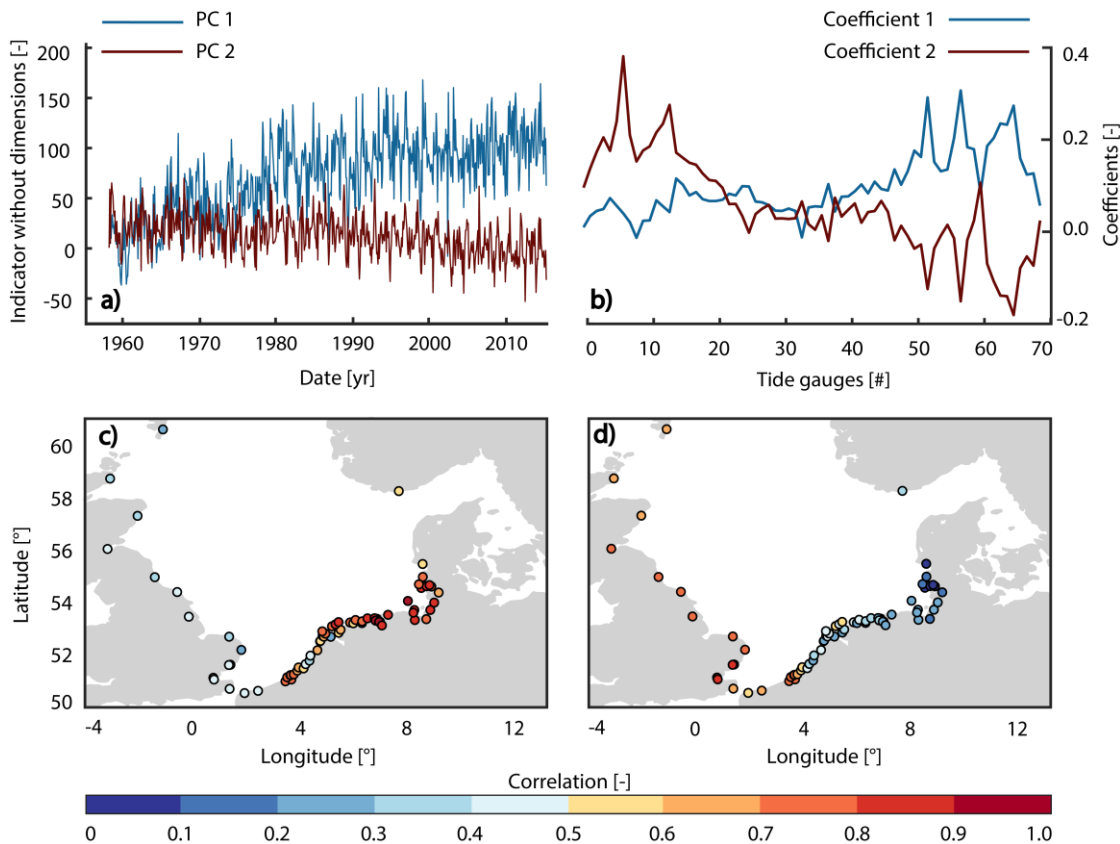
361 Schindelegger et al. (2018) predict an increase in  $M_2$  amplitude in the southwestern part of the  
362 North Sea, between Suffolk/Essex and the Netherlands, while we detect negative trends in  
363 Suffolk/Essex and positive trends in the Netherlands. This disparity could be caused by two  
364 facts: (1) the assumed MSL rise projections used by these studies have not yet occurred and are  
365 therefore theoretical in character, and (2) a contribution of effects not yet considered by  
366 numerical models.

#### 367 **4.2 Principal Components and large-scale effects**

368 Our results of the linear trend analysis point towards a distinct spatial pattern that is occasionally  
369 interrupted by diverging trends at individual locations. To further distinguish between the large-  
370 and small-scale effects of tidal range changes – comprising both trends and short-term variability  
371 – we apply PCA (Figure 6). The first two PCs, which are presented in Figure 6, explain about  
372 69% of the total variance in the entire data set (PC1: 55%, PC2: 14%), while each of the  
373 remaining 68 PCs contributes between 0.01 and 4%. Additionally, no other PC represents  
374 significant parts of the variance at a larger number of tide gauges and is therefore rather local in  
375 character. This indeed suggests that the two leading PCs reflect coherent large-scale effects,  
376 while local effects through anthropogenic interventions are retained in the remainder of the lower  
377 PCs. The amount of these percentages depends to some extent on the spatial distribution of the  
378 tide gauges, which is why it is necessary to consider the PCA results at each tide gauge (Figure  
379 6-c/d, 7d). PC1 describes an increase in tidal range over time, as evident from its positive slope  
380 and the consistently positive values of the associated coefficients at all sites (Figure 6-a). The  
381 magnitudes of the coefficients reveal that the signal represented by PC1 increases as one travels  
382 counterclockwise throughout the basin reaching its strongest expression in the German Bight.  
383 PC2 exhibits a negative trend and is most pronounced in the area of the southeastern coast of the  
384 UK. The coefficients of PC2 change sign from positive values along the UK coast to negative  
385 values in the area of the German Bight (Figure 6-b). Similar to the trends of measured tidal range  
386 (Figure 4), a dipole-like temporal evolution with a node in the area of the English Channel is  
387 detected. In general, PC1 accounts for the increase in tidal range in the German Bight and PC2  
388 represents the decrease in tidal range at the south-eastern coast of the UK. This contrast is also  
389 reflected in the correlation coefficients of the first two PCs with the measured tidal range  
390 changes (a metric that is mostly influenced by inter- and intra-annual variability). Figure 6-c  
391 show moderate but significant correlations of 0.3 – 0.5 for PC1 at the south-western boundary of  
392 the North Sea and displays the highest values ( $\sim 0.9$ ) in the area of the German Bight. A  
393 contrasting picture emerges for PC2. In the area of the German Bight, correlations with tidal  
394 range changes are non-significant and close to zero but almost consistently above 0.7 and  
395 significant in the UK (Figure 6-d).

396  
397 These patterns are also confirmed when considering the explained variance for particular clusters  
398 of tide gauges. Along southeastern UK coastlines, where negative trends are found, the explained  
399 variance of PC1 amounts to only 3%, while PC2 explains about 58% (Table 2). In the

400 Netherlands, the mean explained variance for PC1 is 45% and only 10% for PC2. The  
 401 contribution of the second mode drops to 3% in the German Bight, whereas PC1 explains 77% of  
 402 the variance on average. This spatially reversing pattern is also detectable in the coefficients for  
 403 PC1 and PC2 (Figure 6-b), just as in the linear trends of the tidal range observations. Apparently,  
 404 PC1 with its positive slope is more pronounced in the area of the German Bight, whereas PC2  
 405 (negative slope) dominates in the southeast of the UK. This indicates different underlying  
 406 physical mechanisms for these large-scale signals.

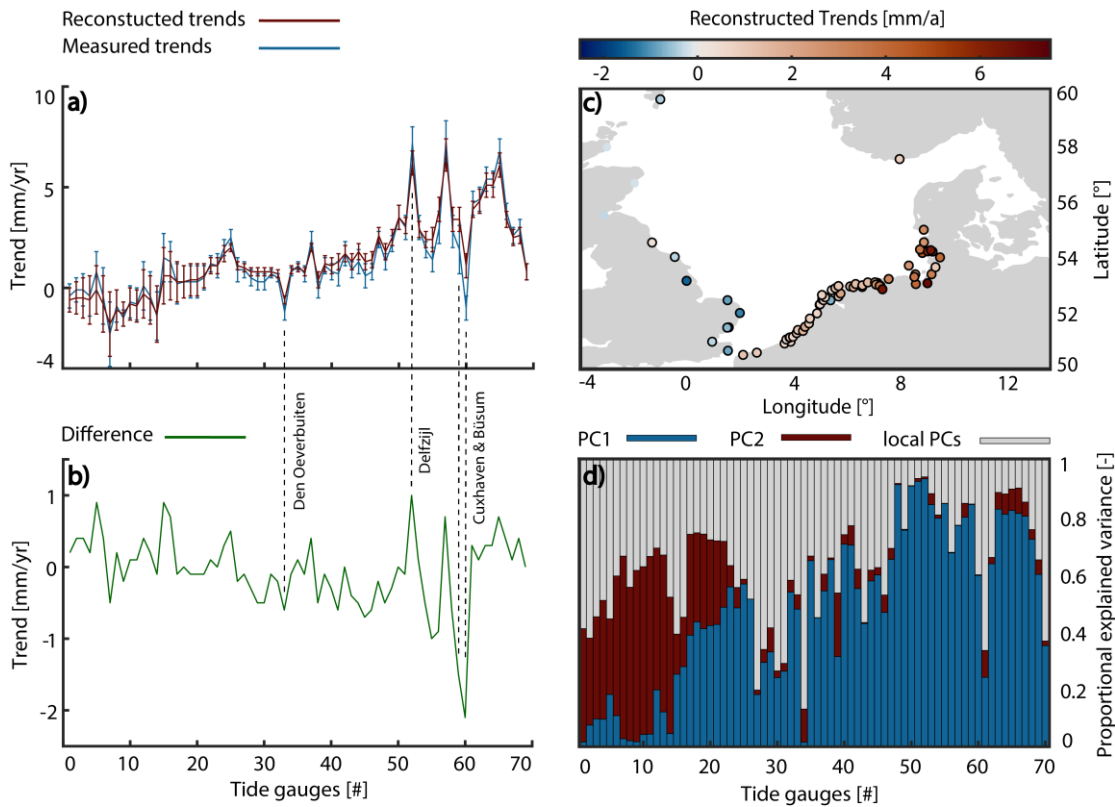


407  
 408 Figure 6: Results of the PCA. (a) Shown are time series of PC1, and PC2 and (b) their corresponding spatial  
 409 patterns. Panels (c) and (d) map the correlations between observations and PC1 (c) and PC2 (d) for each site.

### 410 4.3 Impacts on local tidal range

411 After identifying two large-scale patterns relevant at the majority of tide gauge records in the  
 412 North Sea, we next ask whether we also can identify small-scale effects using the residual signal  
 413 after removing the linearly regressed PC1 and PC2 at individual sites. Figure 7-d shows the  
 414 explained variances and indicates that alongside the described contrast between PC1 and PC2,  
 415 local influences play a major role in some cases. Especially noticeable again are tide gauges Den  
 416 Overbuiten (Netherlands, #33) and Büsum (Germany, #60) due to their high percentage of local  
 417 effects. For example, PC3 (explained overall variance: 4%) captures more than 50% of the  
 418 variance at tide gauge Büsum and around 30% at Cuxhaven (Germany, #59). This anomaly is  
 419 reflected in the comparison of the measured trends with those from re-synthesizing PC1 and PC2

420 (Figure 7-a). The confidence bounds show clear overlaps for most cases, but not at tide gauges  
 421 Den Overbuiten, Büsum, and Cuxhaven. The local characteristics are sufficiently pronounced to  
 422 overshadow the large-scale signals, which is also evident from the difference between measured  
 423 and reconstructed trends in Figure 7-b. In this plot, the 1.0 mm/yr residual at Delfzijl  
 424 (Netherlands, #52) stands out, too. This difference can also be traced back to significant local  
 425 effects, most likely caused by the deepening of the outer areas of the Ems (Hollebrandse,  
 426 (2005)). Hence, local effects have a very large influence on the explained variance at individual  
 427 sites. However, the general trends at most gauges can be qualitatively and quantitatively  
 428 reproduced by PC1 and PC2. Figure 7-c underlines this statement by a spatial map of the  
 429 reconstructed trends, again highlighting the dipole-like pattern between UK and German Bight  
 430 sites. Comparing with the estimates in Section 4.1, the mean trend of tidal range synthesized  
 431 from PC1 and PC2 at the southwest coast of the UK is -1.0 mm/yr, just like the measured trend  
 432 (Table 2). Similar findings apply to the European west coast, where an average reconstructed  
 433 trend of 1.0 mm/yr is achieved compared to 0.8 mm/yr from the in situ data. Local effects  
 434 increase the tidal range by 0.2 mm/yr on average. In the German Bight, the trend from our  
 435 reconstruction is 3.5 mm/yr, overshooting the measured trend by 0.2 mm/yr. Hence, we conclude  
 436 that the opposing trends between the UK and the German Bight are largely controlled by the  
 437 physical processes driving PC1 and PC2.  
 438



439  
 440 Figure 7: Linear trends in tidal range with 95% significance intervals from measurements (blue) and the  
 441 reconstruction (red) based on PC1 and PC2, with the respective difference shown in (b). (c) Spatial distribution of

442 the linear trends from the reconstruction (significant trends outlined) and (d) explained variance of the two PCs as  
 443 share of the total variance

444  
 445

446 Table 2: Measured and reconstructed trends in tidal range and explained variance of the different regions.

Location		Mean Linear Trends [mm/yr]		Explained Variance [%]		
Region	Tide gauges	measured	Reconstructed PC1 and PC2	PC1	PC2	Remaining PCs (local)
Southwestern Coast of GB	Immingham to Dover	-1.0	-1.0	3	58	39
European West Coast	Calais to Huibertgat	0.8	1.0	45	10	45
North Coast of the Netherlands and German Bight	Oude Westereems to Esbjerg	3.3	3.5	77	3	20

447

#### 448 4.4 Identifying physical causes

449 The PCA suggests two modes of variability that appear coherently at the investigated sites in the  
 450 North Sea. Now the question naturally arises whether these signals are produced within or  
 451 outside the basin. If the former is the case, then the corresponding PCs should show no  
 452 correlations to tide gauge records from the adjacent North Atlantic, while an external forcing  
 453 would possibly provide some sort of coherence with those records. No coherence is found for  
 454 PC1 and we therefore conclude that it is produced within the basin, which will be explained later.  
 455 The opposite applies to PC2. A comparison between PC2 and available tide gauge records along  
 456 the European Atlantic coast, Iceland and Canada is shown in Figure 8. Figure 8-c indeed  
 457 documents high and significant correlations of about 0.7 on average between PC2 (calculated  
 458 exclusively on the basis of North Sea data set) and Atlantic tide gauge records spanning the  
 459 region from the English Channel southward to Spain. Moreover, there are significant correlations  
 460 of 0.64 in the north (Reykjavik, Iceland), and even in the Northwest Atlantic (still reaching 0.46  
 461 in Port-aux-Basques, Newfoundland) (Figure 8-a/c). Further south towards the Gulf of Maine,  
 462 these correlations disappear (not shown). A supplemental wavelet analysis (not shown) further  
 463 reveals that the common oscillations between PC2 and the measured tidal range changes mainly  
 464 occur on time scales from 6 to 24 months with particularly high coherence at around 12 months.  
 465 We interpret this finding as an indication for a common high-frequency signal in the North  
 466 Atlantic, causing widespread changes in tidal range.

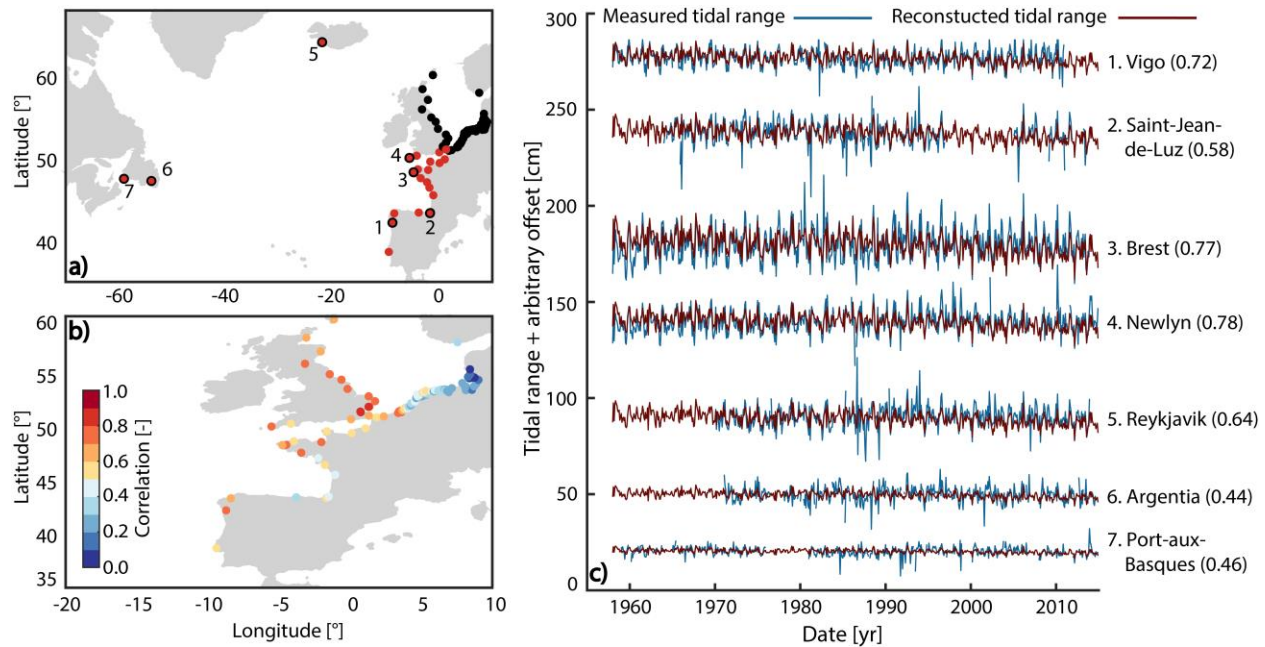
467

468 In order to narrow down the possible causes, outputs from an updated barotropic shallow-water  
 469 model run by Arns et al. (2015a,b) over the period 1958 to 2014 were used. To facilitate a  
 470 rigorous comparison with our in situ data, simulated time series at the locations of the 70 tide  
 471 gauge stations were extracted. A PCA revealed that the PC2 pattern is represented well in the  
 472 simulated data. We find similarly high correlations between the model-based PC and the  
 473 observations of the Atlantic tide gauges. While the mean correlation of the European tide gauge  
 474 records (Figure 8-b) with North Sea PC2 from observations is 0.70 ( $p < 0.05$ ), it is only

475 marginally lower with the barotropic model outputs ( $r=0.66$ ). If the simulated signal is removed  
476 from the model, the correlation becomes insignificant and even disappears at most sites. In  
477 consequence, PC2 must be driven by a process initially included into the boundary conditions  
478 from the numerical model. Since we have used a barotropic formulation without buoyancy  
479 forcing and thermodynamic calculations, we can further infer a purely barotropic relationship.  
480 Amongst the possible relevant factors, the tidal input to the model can safely be neglected. The  
481 DTU10 tide model consists of ten tidal constituents, stationary in time and modulated only by the  
482 18.6-year nodal cycle. The high correlations on the east coast of the UK and in the North  
483 Atlantic are unrelated to this forcing, since purely tide-induced changes would be periodic and  
484 present in the remaining parts of the North Sea.

485  
486 The effects of bottom friction are more involved, but some simple geometric considerations are  
487 instructive. As the tidal wave enters the extensive shallow water areas of the southern North Sea,  
488 energy losses due to friction become dominant, yet the influence of PC2 is increasingly  
489 attenuated in the direction of propagation (Figure 6-d). This discrepancy suggests that frictional  
490 effects do not represent the physical cause of PC2, although they might play a role in suppressing  
491 the magnitude of PC2 in the highly dissipative eastern North Sea region. As our simulations were  
492 performed with an invariant bathymetry and no changes to friction parameters, sea level rise and  
493 meteorological forcing remain as possible causes. We accordingly analyzed correlations between  
494 PC2 and these factors (MSL rise, atmospheric pressure loading, wind velocities and directions)  
495 but could not detect a clear and significant linear relationship. In this context, Arns et al. (2015a)  
496 already referred to the numerous non-linear relationships between the individual parameters in  
497 marginal seas. Specifically, the nonlinear interaction between tide and sea level rise as well as  
498 the dynamic response of the sea surface to meteorological forcing are important (see also Arns et  
499 al., 2020). Further analyses, in particular sensitivity studies taking into account altered tidal  
500 boundary conditions and time variable friction coefficients, will perhaps allow for a final  
501 identification of the ultimate driving factors (e.g., Rasquin et al., 2020).

502



503

504 Figure 8: (a) Extended network of tide gauges with additional stations shown in red, (b) correlations of all tide  
 505 gauges (except 5–7) with PC2 and (c) comparison between measured and reconstructed values of tidal range at the  
 506 newly added tide gauges 1–7. The reconstruction in c) is based on PC2, and the numbers in parentheses indicate the  
 507 respective correlation.

508

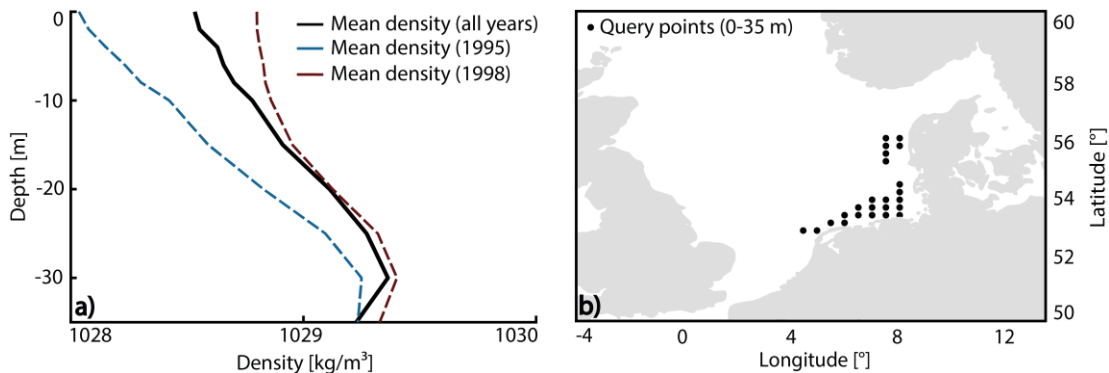
509 While the signal of PC2 is reproducible, PC1 cannot be detected in the simulated data, which  
 510 means PC1 is absent in the barotropic model. At the beginning of this section we stated that there  
 511 is no coherence to the Atlantic tide gauges for PC1, which suggests a origin of the signal within  
 512 the basin. We thus conjecture that a baroclinic, density-related effect inside the North Sea is  
 513 responsible for PC1 and attempt an explanation in terms of known relationships between tidal  
 514 currents and turbulent energy losses in varying stratification conditions. This attribution  
 515 primarily arises from considerations at seasonal time scales. Using hydrographic casts and  
 516 baroclinic model simulations, Müller et al. (2014) linked  $M_2$  elevation changes of 1–5 cm in the  
 517 southern North Sea to the see-sawing of continental shelf stratification between statically stable  
 518 summer and well-mixed winter conditions. Strong buoyancy gradients in mid-depths (20–30 m)  
 519 of shallow waters arise during summer months (see e.g., van Haren et al., 1999) and stabilize the  
 520 water column against energy losses to vertical mixing. The associated increase in barotropic tidal  
 521 transport and surface elevations was found to be most pronounced in very shallow areas and for  
 522 cyclonic rotation of strong tidal currents (Müller, 2012) – conditions that are all present in the  
 523 North Sea.

524

525 To relate at least parts of the PC1 content to this process, we analysed the temporal evolution of  
 526 the North Sea’s density structure based on gridded temperature and salinity profiles from the  
 527 KLIWAS dataset (Bersch et al., 2016). These data are provided as annual values through to 2013  
 528 at comparatively high spatial resolution ( $0.25^\circ \times 0.5^\circ$  latitude-longitude boxes, 2–5 m depth

529 intervals). For consistency, the monthly PC1 series was binned to annual values (1958–2013  
 530 with respect to the length of the KLIWAS dataset) and cleaned from secular changes with  
 531 periods longer than 30 years. Because it is unknown how well KLIWAS represents the smaller,  
 532 more subtle secular trends of density across the water column, we limit our comparison between  
 533 stratification and PC1 to changes on interannual time scales. To suppress noise in the  
 534 climatology, vertical density profiles from a particular set of grid points around the German  
 535 Bight were averaged to a mean water column structure per year (Figure 9). These query points,  
 536 indicated by black dots in Figure 9-b, lie within 2° of 54.5°N/6.0°E and have an exact depth of  
 537 35 m in the KLIWAS dataset. The sampled area is shallow, hosts strong tidal currents, and is not  
 538 permanently mixed, thus favoring a potential effect of stratification on tides. The corresponding  
 539 time-averaged density profile (Figure 9-a) indicates a pycnocline at 20–25 m, conforming in  
 540 principle to modeling results (e.g., Guihou et al., 2018; van Leeuwen et al., 2015). While this  
 541 agreement is reassuring, we also note that our crude spatial averaging ingests profiles in various  
 542 states of stratification (i.e. homogeneous, seasonally or intermittently stratified conditions, see  
 543 Leeuwen et al., 2015). Given the tendency for in situ measurements being taken in summer, the  
 544 KLIWAS dataset may, however, mainly represent the seasonally stratified case.

545



546

547 Figure 9: (a) Vertical profiles of potential density as averaged over all query points in (b) at depths from 0 to 35 m  
 548 for the years 1958 to 2013 (black), the year 1995 (blue) and the years 1998 (red). The two selected years feature the  
 549 greatest deviation from the mean density profile.

550 Some interannual variability in density gradients is already evident from Figure 9-a, where we  
 551 plot individual profiles for the years 1995 and 1998, which differ markedly, by almost 1 kg/m<sup>3</sup>,  
 552 near the surface. An extension to the full depth-time sequence (1958–2013, upper 35 m, see  
 553 Figure 10-a) suggests that fluctuations of this magnitude are common but the density  
 554 perturbations are often mixed throughout the water column, making it difficult to align  
 555 stratification changes in particular years to highs or lows in the PC1 series. We therefore define  
 556 an approximate stability index as top-to-bottom stratification (cf. Eq. 2.9 of Knauss & Garfield,  
 557 2017)

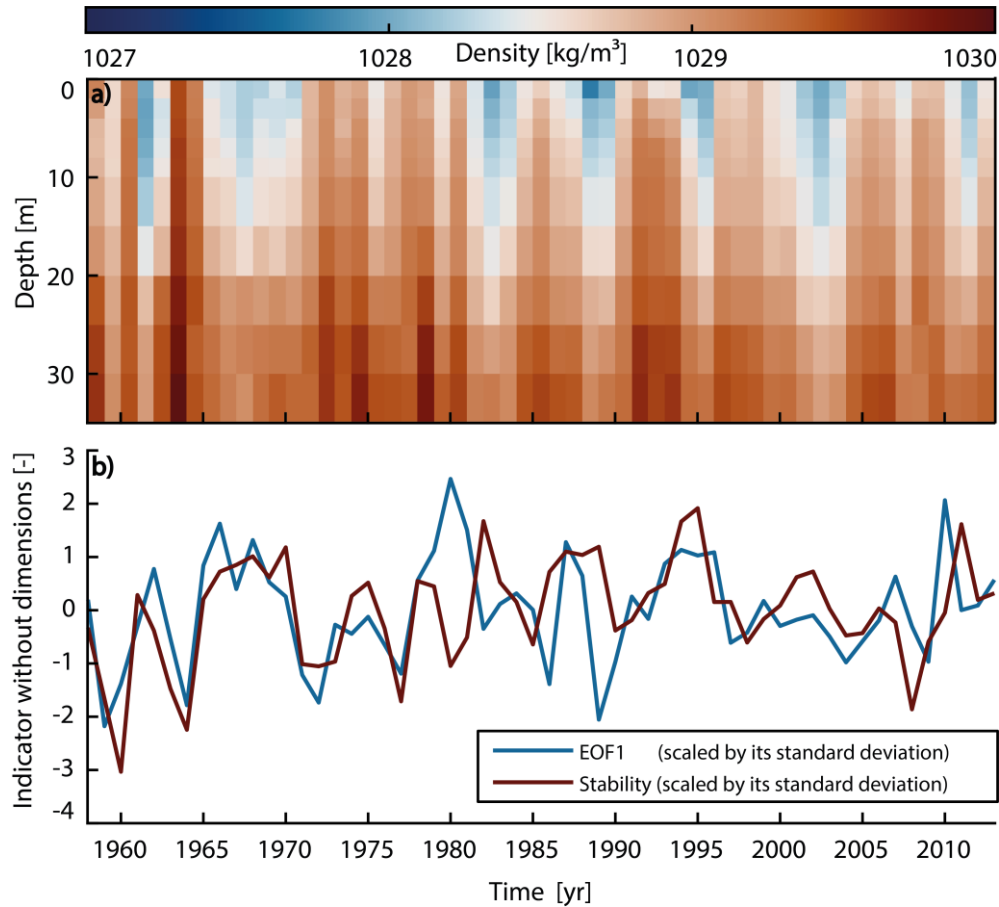
558

$$\text{Stability} = \frac{\rho_{\text{top}} - \rho_{\text{bed}}}{\delta H} \quad (\text{Eq. 3})$$

559

560 where  $\rho_{\text{top}}$  is the averaged density over depths 0, 2 and 4 m,  $\rho_{\text{bed}}$  is a mean density across 25, 30  
561 and 35 m, and  $\delta H = 28$  m. The derived stability index exhibits some noticeably similarity with  
562 interannual tidal range changes in PC1 (Figure 10-b). It closely follows the PC1 curve until  
563 1979, echoes the broad peaks around the years 1987 and 1995, and features multiple reversals in  
564 sign from 2007 onward. Alongside this qualitative agreement, the observed changes in density  
565 gradients amount to about  $0.3 \text{ kg/m}^3$  per 10 m of depth and thus correspond to the order of  
566 magnitude that maintains the seasonal cycle of  $M_2$  in this region (Müller et al., 2014). Therefore,  
567 all indications are that changes to the intensity of summer stratification and/or the time spent in a  
568 stratified (or mixed) regime over the course of a year cause the variance in tidal range  
569 represented by PC1. A breakdown into different modes of stratification variability is tempting  
570 but beyond the scope of our study as it would call for consideration of several factors, including  
571 freshwater buoyancy input, variable local wind stirring, and the inflow of Atlantic water masses  
572 through the northern and southern boundaries (Mathis et al., 2015). Nevertheless, we have  
573 analysed long-term hydrographic data of the North Atlantic and detected high negative  
574 correlations (-0.8) between PC1 and temperature of the upper ocean off the Scottish (down to  
575 about 300 m) and Norwegian coasts (150 m). The anti-correlation is most pronounced in  
576 individual years prior to the 90s and still persists on decadal time scales. This preliminary finding  
577 suggests that a wider North Atlantic scope must be adopted to unravel the origin of the North Sea  
578 tidal range changes and the observed trends in particular.

579



580

581 Figure 10: (a) Spatially averaged density profiles (0–35 m) from the query area in Figure 9-b spanning the period  
 582 1958 to 2013. (b) Comparison between PC1 changes and the stability index (see main text), where both time series  
 583 were scaled by their standard deviation and adjusted for long-term trends.

## 584 **5 Summary and conclusion**

585 We have shown that the tidal range in the southwest and the southeast of the North Sea is  
 586 characterized by a dipole-like pattern between 1958 and 2014, indicating that different forcing  
 587 mechanisms of shelf-wide or larger spatial character may have been present. To separate these  
 588 processes, and treat both trends and short-term variability in a unified framework, a PCA-based  
 589 method was applied to 70 monthly time series of tidal range throughout the North Sea between  
 590 1958 and 2014. Data gaps were filled by the statistical method of Ordinary Kriging. A special  
 591 property of the Kriging procedure is the conservative nature of its estimates at query points,  
 592 resulting in under- rather than an over-estimation of the general system behavior with regard to  
 593 trends and PCs. We were able to detect two large-scale signals and explain about 69% of the  
 594 overall variability in the study area. We attribute the remaining variability of 31% to local  
 595 effects, which vary widely; they may be absent or could well cause over 50% of variability at an  
 596 individual tide gauge. In the overall variance, the maximum contribution of a single local effect  
 597 is at 4%, the average is below 0.4%.

598

599 The second PC represents a large-scale barotropic signal and accounts for the negative trends in  
600 the UK area (up to  $-2.3$  mm/yr). This mode of variability has a North Atlantic extent, as shown  
601 by supplementary analysis of tide gauges in Canada, Reykjavik, and the European Atlantic coast.  
602 Correlations across the basin are high (0.5–0.7) and are caused by common oscillations on time  
603 scales between 6 and 24 months. By detecting the same barotropic signal in the shallow-water  
604 model of Arns et al. (2015a, b), and eliminating suspects that are not part of the model input or  
605 physics, we conclude that only sea level rise and meteorological forcing remain as possible  
606 causes. However, no linear correlations with these parameters were found, implying that non-  
607 linear interactions must be present. A further indication for the presence of shallow water effects  
608 is the severe weakening of the signal as the tidal wave advances from the relative deep water at  
609 the UK into the shallow water areas at the southern and the eastern boundaries of the North Sea

610  
611 The absence of PC1 in the barotropic model and its confinement to the southern North Sea coast  
612 has prompted us to hypothesize that local stratification changes exert a strong influence on the  
613 tidal range in shallow water at various time scales. By analogy to the known seasonal tidal cycle  
614 in the area (Müller et al., 2014), we argue that a stronger pycnocline, possibly lasting over longer  
615 periods, stabilizes the water column against turbulent dissipation and allows for higher tidal  
616 elevations at the coast. The qualitative and quantitative agreement between inter-annual PC1  
617 changes and an empirically derived stability index is certainly tentative, yet it provides an  
618 attractive first-order target for more systematic data analysis and numerical modeling. Further  
619 insight into the nature of large German Bight tidal range changes – particularly the underlying  
620 trends – could be furnished by a regional general circulation model with realistic background  
621 flow and open boundaries to the North Atlantic.

## 622 **Acknowledgments:**

623 The analyses performed here were part of the DFG-funded project TIDEDYN (*Analyzing long*  
624 *term changes in the tidal dynamics of the North Sea*, project number 290112166) and the BMBF-  
625 funded project ALADYN (*Analyzing long-term changes of tidal dynamics in the German Bight*,  
626 Subproject A, BMBF 03F0756A). Michael Schindelegger acknowledges financial support made  
627 available by the Austrian Science Fund (FWF, project P30097-N29).

628  
629 Data from GESLA (Global Extreme Sea Level Analysis, GESLA, Woodworth et al. 2017), Open  
630 Earth (Deltares, [http://opendap.deltares.nl/thredds/catalog/opendap/rijkswaterstaat/waterbase/27\\_](http://opendap.deltares.nl/thredds/catalog/opendap/rijkswaterstaat/waterbase/27_Waterhoogte_in_cm_t.o.v._normaal_amsterdams_peil_in_oppervlaktewater/nc/catalog.html)  
631 [Waterhoogte\\_in\\_cm\\_t.o.v.\\_normaal\\_amsterdams\\_peil\\_in\\_oppervlaktewater/nc/catalog.html](http://opendap.deltares.nl/thredds/catalog/opendap/rijkswaterstaat/waterbase/27_Waterhoogte_in_cm_t.o.v._normaal_amsterdams_peil_in_oppervlaktewater/nc/catalog.html)) and  
632 the responsible German authorities (Wasser- und Schifffahrtsverwaltung des Bundes via the  
633 portals of the associated Central Data Management, ZDM, <https://www.portalnsk.de>) were used.

## 634 **References**

635 Arns, A., Wahl, T., Dangendorf, S., & Jensen J. (2015a). The impact of sea level rise on storm  
636 surge water levels in the northern part of the German Bight. *Coastal Engineering*, 96,  
637 118–131. <https://doi.org/10.1016/j.coastaleng.2014.12.002>

638

639 Arns, A., Wahl, T., Haigh, I., & Jensen J. (2015b). Determining return water levels at ungauged  
640 coastal sites: a case study for northern Germany. *Ocean Dynamics*, 65 (4), S. 539–554.  
641 <https://doi.org/10.1007/s10236-015-0814-1>.

642

643 Arns, A., Wahl, T., Wolff, C., Vafeidis, A. T., Haigh, I. D., Woodworth, P., Niehüser, S., &  
644 Jensen, J. (2020). Non-linear interaction modulates global extreme sea levels, coastal  
645 flood exposure, and impacts. *Nature Communications*, 11, 1918(2020).  
646 <https://doi.org/10.1038/s41467-020-15752-5>

647

648 Becker, J. J., Sandwell, D.T., Smith, W. H. F., Braud, J., Binder, B., Depner, J., Fabre, D.,  
649 Factor, J., Ingalls, S., Kim, S-H., Ladner, R., Marks, K., Nelson, S., Pharaoh, A.,  
650 Trimmer, R., von Rosenberg, J., Wallace, G., & Weatherall, P. (2009). „Global  
651 Bathymetry and Elevation Data at 30 Arc Seconds Resolution: SRTM30\_PLUS“. *Marine*  
652 *Geodesy* 32(4), 355–371. <https://doi.org/10.1080/01490410903297766>

653

654 Bersch, M., Hinrichs, I., Gouretski, V., & Sadikni, R. (2016). Hydrographic climatology of the  
655 North Sea and surrounding regions – version 2.0, Center for Earth System Research and  
656 Sustainability (CEN), University of Hamburg, [icdc.cen.uni-](http://icdc.cen.uni-hamburg.de/daten/ocean/knsc-hydrographic.html)  
657 [hamburg.de/daten/ocean/knsc-hydrographic.html](http://icdc.cen.uni-hamburg.de/daten/ocean/knsc-hydrographic.html)

658

659 Cheng, Y., & Andersen, O. B. (2010). Improvement in global ocean tide model in shallow water  
660 regions. Poster, SV.1-68 45, OSTST, Lisbon, Oct.18-22.

661

662 Codiga, D. L. (2011). Unified tidal analysis and prediction using the UTide Matlab functions.  
663 Technical Report 2011-01. Graduate School of Oceanography, University of Rhode  
664 Island, Rhode Island. <https://doi.org/10.13140/RG.2.1.3761.2008>

665

666 Compo, G. P., Whitaker, J. S., Sardeshmukh, P. D., Matsui, N., Allan, R. J., Yin, X., Gleason, B.  
667 E., Vose, R. S., Rutledge, G., Bessemoulin, P., Brönnimann, S., Brunet, M., Crouthamel,  
668 R. I., Grant, A. N., Groisman, P. Y., Jones, P. D., Kruk, M. C., Kruger, A. C., Marshall,  
669 G. J., Maugeri, M., Mok, H. Y., Nordli, Ø., Ross, T. F., Trigo, R. M., Wang, X. L.,  
670 Woodruff, S. D., & Worley, S. J. (2011). The Twentieth Century Reanalysis Project.  
671 *Quarterly Journal of the Royal Meteorological Society*, 137, 1-28.  
672 <https://doi.org/10.1002/qj.776>.

673

674 Cowtan, K., & Way, R. G. (2014). Coverage bias in the HadCRUT4 temperature series and its  
675 impact on recent temperature trends. *Quarterly Journal of the Royal Meteorological*  
676 *Society*, 140, 1935-1944. <https://doi.org/10.1002/qj.2297>

677

- 678 Cressie, N. (1990). The origins of kriging. *Mathematical Geology*, 22, 239–252.  
679 <https://doi.org/10.1007/BF00889887>  
680
- 681 Dangendorf, S., Marcos, M., Müller, A., Zorita, E., Riva, R., Berk, K., & Jensen, J. (2015).  
682 Detecting anthropogenic footprints in sea level rise. *Nature Communications*, 6, 7849.  
683 <https://doi.org/10.1038/ncomms8849>  
684
- 685 Dangendorf, S., Hay, C., Calafat F. M., Marcos, M., Piecuch, C. G., Berk, K. & Jensen, J.  
686 (2019). Persistent acceleration in global sea-level rise since the 1960s, *Nature Climate*  
687 *Change*, 9, 705-710. <https://doi.org/10.1038/s41558-019-0531-8>  
688
- 689 Devlin A.T., Jay D.A., Talke S.A. and Zaron E. (2014). Can tidal perturbations associated with  
690 sea level variations in the western Pacific Ocean be used to understand future effects of  
691 tidal evolution?. *Ocean Dynamics*, 64(8), 1093–1120, [https://doi.org/10.1007/s10236-](https://doi.org/10.1007/s10236-014-0741-6)  
692 [014-0741-6](https://doi.org/10.1007/s10236-014-0741-6)  
693
- 694 DIN 4049-3 (1994). Hydrologie, Teil 3: Begriffe zur quantitativen Hydrologie. ICS 07.060;  
695 01.040.07  
696
- 697 Doodson, A.T. (1924). Perturbations of harmonic tidal constants. *Proceedings of the Royal*  
698 *Society*, 106, 513-526, <https://doi.org/10.1098/rspa.1924.0085>  
699
- 700 Feng, X., Tsimplis, M.N., & Woodworth, P.L. (2015). Nodal variations and long-term changes in  
701 the main tides on the coasts of China. *Journal of Geophysical Research: Oceans*, 120(2),  
702 1215–1232. <https://doi.org/10.1002/2014JC010312>  
703
- 704 Flick, R.E., Murray, J.F., & Ewing, L.C. (2003). Trends in United States Tidal Datum Statistics  
705 and Tide Range. *Journal of Waterway, Port, Coastal, and Ocean Engineering*, 129(4),  
706 155–164, [https://doi.org/10.1061/\(ASCE\)0733-950X\(2003\)129:4\(155\)](https://doi.org/10.1061/(ASCE)0733-950X(2003)129:4(155))  
707
- 708 Fühnböter, A., & Jensen, J. (1985). Säkularänderungen der mittleren Tidewasserstände in der  
709 Deutschen Bucht. *Die Küste*, 42, 78-100  
710
- 711 Grinsted, A., Moore, J. C., & Jevrejeva, S. (2004). Application of the cross wavelet transform  
712 and wavelet coherence to geophysical time series. *Nonlinear Processes in Geophysics*,  
713 11, 561-566. <https://doi.org/10.5194/npg-11-561-2004>  
714
- 715 Guihou, K., Polton, J., Harle, J., Wakelin, S., O’Dea, E. & Holt, J. (2017). Kilometric Scale  
716 Modeling of the North West European Shelf Seas: Exploring the Spatial and Temporal

- 717 Variability of Internal Tides. *Journal of Geophysical Research: Oceans*, 123(1).  
718 <https://doi.org/10.1002/2017JC012960>  
719
- 720 Haigh, I. D. (2017). Tides and Water Levels. *Encyclopedia of Maritime and Offshore*  
721 *Engineering*, 248, 1–13  
722
- 723 Haigh, I. D., Pickering, M. D., Green, J. A. M., Arbic, B. K., Arns, A., Dangendorf, S., Hill D.,  
724 Horsburgh, K., Howard, T., Idier, D., Jay, D. A., Jänicke, L., Lee, S. B., Müller, M.,  
725 Schindelegger, M., Talke, S. A., Wilmes, S.-B., & Woodworth P. L. (2020). The Tides  
726 They Are a-Changin’: A comprehensive review of past and future non-astronomical  
727 changes in tides, their driving mechanisms and future implications. *Review of*  
728 *Geophysics*, 58(1), <https://doi.org/10.1029/2018RG000636>.  
729
- 730 Hollebrandse, F. A. P. (2005). Temporal development of the tidal range in the southern North  
731 Sea. *Dissertation*, Faculty of Civil Engineering and Geosciences, TU Delft; 2005.  
732
- 733 Horsburgh, K. J., & Wilson, C. (2007). Tide-surge interaction and its role in the distribution of  
734 surge residuals in the North Sea. *Journal of Geophysical Research*, 112.  
735 <https://doi.org/10.1029/2006JC004033>  
736
- 737 Huthnance, J. M. (1991). Physical Oceanography of the North Sea, *Ocean & Shoreline*  
738 *Management*. 16, 199-231. [https://doi.org/10.1016/0951-8312\(91\)90005-M](https://doi.org/10.1016/0951-8312(91)90005-M)  
739
- 740 Idier, D., Paris, F., Cozannet, G. L., Boulahya, F., & Dumas, F. (2017). Sea-level rise impacts on  
741 the tides of the European Shelf. *Continental Shelf Research*, 137, 56-71.  
742 [doi:10.1016/j.csr.2017.01.007](https://doi.org/10.1016/j.csr.2017.01.007)  
743
- 744 Jay, D. A. (2009). Evolution of tidal amplitudes in the eastern Pacific Ocean. *Geophysical*  
745 *Research Letters*, 36(4). <https://doi.org/10.1029/2008GL036185>  
746
- 747 Jensen, J., Dangendorf, S., Wahl, T., & Steffen, H. (2014). Meeresspiegeländerungen in der  
748 Nordsee: Vergangene Entwicklungen und zukünftige Herausforderungen mit einem  
749 Fokus auf die Deutsche Bucht. *Hydrologie und Wasserbewirtschaftung*, 58(4), 304–323.  
750 [https://doi.org/10.5675/HyWa\\_2014,6\\_1](https://doi.org/10.5675/HyWa_2014,6_1)  
751
- 752 Jensen, J. (2020). Retrospektive der Meeresspiegelforschung in Deutschland. *Hydrografische*  
753 *Nachrichten*, 115, 18-26. <https://doi.org/10.23784/HN115-03>  
754
- 755 Jolliffe, I. T. (2002). *Principal Component Analysis*, Springer Series in Statistics, Springer, New  
756 York. <https://doi.org/10.1007/b98835>

- 757  
758 Keller, H. (1901). *Weser und Ems, ihre Stromgebiete und ihre wichtigsten Nebenflüsse: eine*  
759 *hydrographische, wasserwirtschaftliche und wasserrechtliche Darstellung*, Verlag von  
760 Dietrich Reimer, Berlin  
761
- 762 Knauss, J. A., & Garfield, N. (2017). *Introduction to Physical Oceanography*. *Waveland Press*,  
763 3<sup>rd</sup> Edition, ISBN 147863250X, 978-1-4786-3250-4.  
764
- 765 Krige, D. G. (1951). A statistical approach to some basic mine valuation problems on the  
766 Witwatersrand. *Journal of the Southern African Institute of Mining and Metallurgy*, 52,  
767 119 – 139  
768
- 769 Mathis, M., Elizalde, A., Mikolajewicz, U., & Pohlmann, T. (2015). Variability patterns of the  
770 general circulation and sea water temperature in the North Sea, *Progress in*  
771 *Oceanography*, 135, 91-112. <https://doi.org/10.1016/j.pocean.2015.04.009>  
772
- 773 Mawdsley, R. J., Haigh, I. D., & Wells, N. C. (2015). Global secular changes in different tidal  
774 high water, low water and range levels. *Earth's Future*, 3(2), 66–81.  
775 <https://doi.org/10.1002/2014EF000282>  
776
- 777 Mawdsley, R. J., & Haigh, I. D. (2016). Spatial and Temporal Variability and Long-Term Trends  
778 in Skew Surges Globally. *Frontiers in Marine Science*, 3:29.  
779 <https://doi.org/10.3389/fmars.2016.00029>  
780
- 781 Müller, M., Arbic, B., & Mitrovica, J.X. (2011). Secular trends in ocean tides: observations and  
782 model results. *Journal of Geophysical Research*, 116  
783 <https://doi.org/10.1029/2010JC006387>  
784
- 785 Müller, M. (2011). Rapid change in semi-diurnal tides in the North Atlantic since 1980.  
786 *Geophysical Research Letters*, 48, 107-118. <https://doi.org/10.1029/2011GL047312>  
787
- 788 Müller, M. (2012). The influence of stratification conditions on barotropic tidal transport and its  
789 implication for seasonal and secular changes of tides. *Continental Shelf Research*, 47,  
790 107-118. <https://doi.org/10.1016/j.csr.2012.07.003>  
791
- 792 Müller, M., Cherniawsky, J., Foreman, M., & von Storch, J.-S. (2014). Seasonal variation of the  
793 M2 tide. *Ocean Dynamics*, 64(2), 159–177. <https://doi.org/10.1007/s10236-013-0679-0>  
794
- 795 Oppenheimer, M., Glavovic, B., Hinkel, J., Van de Wal, R. S. W., Magnan, A. K., Abd-Elgawad,  
796 A., Cai, R., Cifuentes-Jara, M., DeConto, R. M., Ghosh, T., Hay, J., Isla, F., Marzeion,

- 797 B., Meyssignac, B. & Sebesvari, Z. (2019). Sea level rise and implications for low lying  
798 Islands, coasts and communities. *IPCC special report on the ocean and cryosphere in a*  
799 *changing climate*, Cambridge University Press, Cambridge, UK  
800
- 801 Prandle, D., & Wolf, J. (1978). The interaction of surge and tide in the North Sea and River  
802 Thames. *Journal of the Royal Astronomical Society*, 55. [https://doi.org/10.1111/j.1365-](https://doi.org/10.1111/j.1365-246X.1978.tb04758.x)  
803 [246X.1978.tb04758.x](https://doi.org/10.1111/j.1365-246X.1978.tb04758.x)  
804
- 805 Proudman, J., & Doodson, A.T. (1924). The principal constituent of the tides of the North Sea.  
806 *Philosophical Transactions of the Royal Society*, 224, 616-625.  
807 <https://doi.org/10.1098/rsta.1924.0005>  
808
- 809 Pickering, M. D., Wells, N. C., Horsburgh, K. J., & Green, J. A. M. (2012). The impact on the  
810 European Shelf tides by future sea-level rise. *Continental Shelf Research*, 35, 1-15.  
811 <https://doi.org/10.1016/j.csr.2011.11.011>  
812
- 813 Pugh, D., & Woodworth, P. (2014). Sea-level science: Understanding tides, surges, tsunamis and  
814 mean sea-level changes. Cambridge University Press, Cambridge  
815
- 816 Quante, M., & Colijn, F. (2016). North Sea Region Climate Change Assessment. Springer  
817 Nature, New York. <https://doi.org/10.1007/978-3-319-39745-0>  
818
- 819 Rasquin, C., Seiffert, R., Wachler, B., & Winkel, N. (2020). The significance of coastal  
820 bathymetry representation for modelling the tidal response to mean sea level rise in the  
821 German Bight. *Ocean Science*, 16, 31-44. <https://doi.org/10.5194/os-16-31-2020>  
822
- 823 Ray, R. D. (2009). Secular changes in the solar semidiurnal tide of the western North Atlantic  
824 Ocean. *Geophysical Research Letters*, 36. <https://doi.org/10.1029/2009GL040217>  
825
- 826 Ray, R. D., & Talke, S. A. (2019). Nineteenth-Century Tides in the Gulf of Maine and  
827 Implications for Secular Trends. *Journal of Geophysical Research Oceans*, 124,  
828 <https://doi.org/10.1029/2019JC015277>  
829
- 830 Rigor, I. G., Colony, R. L., & Martin, S. (2000). Variations in surface air temperature  
831 observations in the arctic. *Journal of Climate*, 13, 1979-1997.  
832 [https://doi.org/10.1175/1520-0442\(2000\)013<0896:VISATO>2.0.CO;2](https://doi.org/10.1175/1520-0442(2000)013<0896:VISATO>2.0.CO;2)  
833
- 834 Rohde, R. A., Muller, R. A., Jacobsen, R., Perlmutter, S., Rosenfeld, A., Wurtele, J., Curry, J.,  
835 Wickham, C., & Mosher, S. (2013). Berkeley earth temperature averaging process.  
836 *Geoinformatics & Geostatistics: An Overview*. <http://dx.doi.org/10.4172/gigs.1000103>

- 837  
838 Schindelegger, M., Green, J. A. M., Wilmes, S.-B., & Haigh, I.D. (2018). Can we model the  
839 effect of observed sea level rise on tides?. *Journal of Geophysical Research: Oceans*,  
840 123, 4593-4609. <https://doi.org/10.1029/2018JC013959>  
841
- 842 Schrottke, K., & Heyer, H. (2013). Aufbau von integrierten Modellsystemen zur Analyse der  
843 langfristigen Morphodynamik in der Deutschen Bucht: AufMod. *Bundesamt für*  
844 *Seeschifffahrt und Hydrographie*. <https://doi.org/10.2314/GBV:780783271>  
845
- 846 Schwanghart, W. (2020). Ordinary Kriging  
847 <https://www.mathworks.com/matlabcentral/fileexchange/29025-ordinary-kriging>),  
848 MATLAB Central File Exchange. Retrieved February 25, 2020.  
849
- 850 Sündermann, J. & Pohlmann, T. (2011). A brief analysis of North Sea physics. *Oceanologia*,  
851 53(3), 663-689. <https://doi.org/10.5697/oc.53-3.663>  
852
- 853 Talke, S. A., & Jay, D. A. (2017). Archival Water-Level Measurements: Recovering Historical  
854 Data to Help Design for the Future, *US Army Corps of Engineers: Civil Works Technical*  
855 *Series*, 412, Report CWTS-02  
856
- 857 Talke, S. A. & Jay D. A. (2020). Changing Tides: The Role of Natural and Anthropogenic  
858 Factors, *Annual Review of Marine Science*, 12:121-151, [https://doi.org/10.1146/annurev-](https://doi.org/10.1146/annurev-marine-010419-010727)  
859 [marine-010419-010727](https://doi.org/10.1146/annurev-marine-010419-010727)  
860
- 861 Taylor, G. I. (1922): Tidal Oscillations in Gulfs and Rectangular Basins. *Proceedings of the*  
862 *London Mathematical Society*, s2-20(1), 148–181. [https://doi.org/10.1112/plms/s2-](https://doi.org/10.1112/plms/s2-20.1.148)  
863 [20.1.148](https://doi.org/10.1112/plms/s2-20.1.148)  
864
- 865 Van Haren, H., Maas, L., Zimmerman, J. T. F., Ridderinkhof, H., & Malschaert, H. (1999).  
866 Strong inertial currents and marginal internal wave stability in the central North Sea,  
867 *Geophysical Research Letters*, 26(19), <https://doi.org/10.1029/1999GL002352>  
868
- 869 Van Leeuwen, S., Tett, P., Mills, D., & van der Molen, J. (2015). Stratified and nonstratified  
870 areas in the North Sea: Long-term variability and biological and policy implications.  
871 *Journal of Geophysical Research: Oceans*, 120(7),  
872 <https://doi.org/10.1002/2014JC010485>  
873

- 874 Wahl, T., Haigh, I. D., Woodworth, P. L., Albrecht, F., Dillingh, D., Jensen, J., Nicholls, R. J.,  
875 Weisse, R., & Wöppelmann, G. (2013). Observed mean sea level changes around the  
876 North Sea coastline from 1800 to present. *Earth-Science Reviews*, 124, 51–67.  
877 <https://doi.org/10.1016/j.earscirev.2013.05.003>.  
878
- 879 Woodworth, P. L., Shaw, S. M., & Blackman, D. L. (1991). Secular trends in mean tidal range  
880 around the British Isles and along the adjacent European coastline. *Geophysical Journal*  
881 *International*, 104(3), 593–609. <https://doi.org/10.1111/j.1365-246X.1991.tb05704.x>  
882
- 883 Woodworth, P. (2010). A survey of recent changes in the main components of the ocean tides.  
884 *Continental Shelf Research*, 30, 1680-1691. <https://doi.org/10.1016/j.csr.2010.07.002>  
885
- 886 Woodworth, P., Hunter, J. R., Marcos, M., Caldwell, P., Menedez, M., & Haigh, I. D. (2017).  
887 Towards a global higher-frequency sea level dataset. *Geoscience Data Journal*, 3(2), 50-  
888 59. <https://doi.org/10.1002/gdj3.42>